

Distributed Irregular Codes Relying on Decode-and-Forward Relays as Code Components

Soon Xin Ng, *Senior Member, IEEE*, Yonghui Li, *Senior Member, IEEE*,
Branka Vucetic, *Fellow, IEEE*, and Lajos Hanzo, *Fellow, IEEE*

Abstract—A near-capacity distributed coding scheme is conceived by incorporating multiple relay nodes (RNs) for constructing a virtual irregular convolutional code (IRCC). We first compute the relay channel's capacity and then design IRCCs for the source and relay nodes. Extrinsic information transfer (EXIT) charts are utilized to design the codes for approaching the achievable capacity of the relay channels. Additionally, we improve the transmit power efficiency of the overall system by invoking both power allocation and relay selection. We found that even a low-complexity repetition code or a unit-memory convolutional code is capable of forming a near-capacity virtual IRCC. The performance of the proposed distributed IRCC (DIRCC) scheme is shown to be perfectly consistent with that predicted from the EXIT chart. More specifically, the DIRCC scheme is capable of operating within 0.68 dB from the corresponding lower bound of the relay channel capacity, despite the fact that each RN is exposed to realistic decoding errors due to communicating over imperfect source-relay channels.

Index Terms—Cooperative communications, cooperative diversity, distributed coding, irregular convolutional codes (IRCCs), relay selection.

I. INTRODUCTION

MULTIPLE-input multiple-output (MIMO) techniques [1], [2], which employ multiple antennas at both the transmitter and the receiver, are capable of providing reliable transmissions at high data rates or at low transmit power. However, the correlation of signals transmitted from a small mobile unit equipped with multiple antennas degrades the attainable performance. As a remedy, cooperative communications [3], [4] constitutes an attractive solution by forming a distributed MIMO system with the aid of user cooperation, where each user node may be equipped with just a single antenna. More explicitly, user cooperation is invoked for the sake of achieving reliable and efficient transmission. The broadcast nature of wireless transmission makes reception at relay terminals possible at

Manuscript received April 11, 2014; revised September 22, 2014; accepted November 10, 2014. Date of publication December 5, 2014; date of current version October 13, 2015. This work was supported in part by the International Visiting Research Fellowship scheme (2010) from the University of Sydney, by the European Union's Seventh Framework Programme (FP7/2007-2013) under the auspices of the CONCERTO project (Grant 288502), and by the European Research Council's Advanced Fellow Grant. The review of this paper was coordinated by Prof. S. Muhaidat.

S. X. Ng and L. Hanzo are with the School of Electronics and Computer Science, University of Southampton, Southampton SO17 1BJ, U.K. (e-mail: sxn@ecs.soton.ac.uk; lh@ecs.soton.ac.uk).

Y. Li and B. Vucetic are with the School of Electrical and Information Engineering, University of Sydney, Sydney, N.S.W. 2006, Australia (e-mail: yonghui.li@sydney.edu.au; branka.vucetic@sydney.edu.au).

Color versions of one or more of the figures in this paper are available online at <http://ieeexplore.ieee.org>.

Digital Object Identifier 10.1109/TVT.2014.2370737

no extra cost. Furthermore, relaying typically benefits from a reduced path loss, which makes cooperative communications power efficient. The most popular cooperative protocols are the decode-and-forward (DAF) and the amplify-and-forward (AAF) schemes. However, a strong channel code is required for mitigating potential error propagation in the DAF scheme or for avoiding noise enhancement of the AAF scheme.

Distributed coding [5], which involves joint coding design between the source node (SN) and relay nodes (RNs), is one of the promising coding techniques conceived for approaching the achievable capacity of the relay channel with the aid of iterative detection at the destination node (DN). More specifically, distributed turbo codes [6]–[9], distributed low-density parity-check codes [10]–[12], distributed turbo trellis coded modulation [13], distributed space-time codes [14]–[17], distributed self-concatenated convolutional codes [18], distributed rateless codes [19], and distributed soft coding [20] have been proposed for cooperative communications. Furthermore, selecting beneficial RNs that exhibit high-quality source-to-relay and relay-to-destination links is capable of significantly reducing the overall transmission power of the relay network [21], [22]. On the other hand, irregular convolutional codes (IRCCs) [23], [24] constitute a powerful outer code family conceived for assisting serially concatenated channel coding schemes in approaching the corresponding channel capacity [25]–[27]. More explicitly, $K \geq 1$ out of N component codes are chosen to produce an encoded sequence having a length of N_c bits. The p th subcode produces a subsequence having a length of $\alpha_p N_c$ bits, where α_p is the p th IRCC weighting coefficient. The K component codes and their weighting coefficients are chosen to create an IRCC extrinsic information transfer (EXIT) [23], [28] curve for matching that of the inner code. Near-capacity performance is achieved, when the area between the inner and outer code's EXIT curves is minimized.

In this contribution, we propose a distributed IRCC (DIRCC) scheme, where the IRCC component codes are distributed to appropriately selected RNs, for the sake of approaching the relay channel capacity. First, an IRCC is designed at the SN for approaching the capacity of the source-to-relay links. Then, K RNs are chosen to form a virtual K -component IRCC for approaching the overall relay channel capacity. Iterative decoding is performed at all RNs and DN. As another potential benefit, the specific RNs that have more battery charge may be used for encoding and transmitting the longer bit sequences, whereas those having limited power can be invoked for encoding and relaying shorter bit sequences. Hence, the required processing and transmission power can be distributed to RNs having

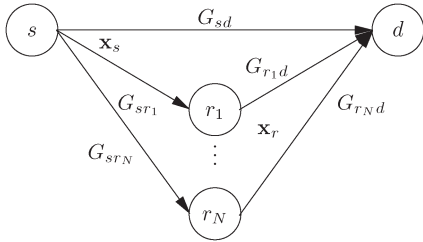


Fig. 1. Schematic of the DIRCC scheme.

different power constraints, instead of heavily exploiting a single RN during the entire DAF process. This is particularly beneficial when energy-harvesting nodes (EHNs) [29] are utilized as our RNs. More explicitly, there may be several EHNs available that have sufficient battery charge for carrying out partial encoding while there may not be a single EHN that has the battery charge required to carry out the entire IRCC encoding. Both relay selection and power allocation are also considered for improving the transmission power efficiency of the overall system.

The rest of this paper is organized as follows. The system model is described in Section II, whereas the system design is detailed in Section III. Our simulation results are discussed in Section IV, whereas our conclusions are offered in Section V.

II. SYSTEM MODEL

We considered a two-hop half-duplex relaying model, involving a single SN, multiple RNs, and a DN. The schematic of the proposed DIRCC scheme is shown in Fig. 1, where the SN s broadcasts a frame of coded symbols \mathbf{x}_s during the first transmission phase T_1 , which is received by the DN d and all the RNs. The carefully selected K out of N RNs decode \mathbf{x}_s and reencode a portion of the decoded bits to form the virtual IRCC coded symbols $\mathbf{x}_r = [\mathbf{x}_{r_1} \ \mathbf{x}_{r_2} \ \dots \ \mathbf{x}_{r_k} \ \dots \ \mathbf{x}_{r_K}]$, where the subsequence \mathbf{x}_{r_k} is transmitted by the k th RN, r_k , during the k th timeslot of the second transmission phase T_2 . Each selected RN transmits its encoded symbol sequence in different timeslots¹ to the DN.

The j th signal received at the RN during T_1 , when N_s symbols are transmitted from the SN, can be written as

$$y_{r_k,j}^{(T_1)} = \sqrt{G_{sr_k}} h_{sr_k,j}^{(T_1)} x_{s,j} + n_{r_k,j}^{(T_1)} \quad (1)$$

where $j \in \{1, \dots, N_s\}$, and $h_{ab,j}^{(T_l)}$ is the complex-valued fast Rayleigh fading channel coefficient between node a and node b at instant j during the l th transmission phase T_l , whereas $n_{b,j}^{(T_l)}$ is zero-mean complex additive white Gaussian noise at node b having a variance of $N_0/2$ per dimension during T_l . Note that we consider a free-space path-loss model having a path-loss exponent of 2. Hence, the reduced-distance-related path-loss reduction (or geometrical gain) of the SN-to-RN link with respect to the SN-to-DN link [6], [18], [30] is given by

$$G_{sr_k} = \left(\frac{d_{sd}}{d_{sr_k}} \right)^2 \quad (2)$$

¹It is possible to extend the scheme to have simultaneous transmissions from all RNs at the cost of more complex detection at the DN.

where d_{ab} stands for the distance between node a and node b . Similarly, the j th signal received at the DN during T_1 can be expressed as

$$y_{d,j}^{(T_1)} = \sqrt{G_{sd}} h_{sd,j}^{(T_1)} x_{s,j} + n_{d,j}^{(T_1)} \quad (3)$$

where we have $G_{sd} = 1$. Each RN decodes the received signal for retrieving the original information sequence. Only a portion of the information sequence is reencoded at each RN using the corresponding component encoder for transmission to the DN.

The j th symbol from the k th RN received at the DN during the second transmission phase T_2 can be written as

$$y_{r_k,d,j}^{(T_2)} = \sqrt{G_{r_k,d}} h_{r_k,d,j}^{(T_2)} x_{r_k,j} + n_{d,j}^{(T_2)} \quad (4)$$

where the modulated symbol sequence of the k RN is given by $\mathbf{x}_{r_k} = [x_{r_k,1} \ \dots \ x_{r_k,j} \ \dots \ x_{r_k,L_k}]$, L_k is the number of modulated symbols, and the geometrical gain of the RN-to-DN link with respect to the SN-to-DN link is given by

$$G_{r_k,d} = \left(\frac{d_{sd}}{d_{r_k,d}} \right)^2. \quad (5)$$

The total number of coded symbols of the virtual IRCC formed by the K RNs is given by

$$N_r = \sum_{k=1}^K L_k. \quad (6)$$

In general, each RN will transmit a different number of coded and modulated symbols, i.e., $L_k \neq L_p$ for $k \neq p$.

If $x_{a,j}$ is the j th symbol transmitted from node a , the average receive signal-to-noise power ratio (SNR) at node b is given by

$$\Gamma_r = \frac{\mathbb{E}\{G_{ab}\} \mathbb{E}\{|h_{ab,j}|^2\} \mathbb{E}\{|x_{a,j}|^2\}}{N_0} = \frac{G_{ab}}{N_0} \quad (7)$$

where $\mathbb{E}\{|h_{ab,j}|^2\} = 1$ when communicating over fast Rayleigh fading channels and $\mathbb{E}\{|x_{a,j}|^2\} = 1$. For convenience, we define the average *transmit SNR* as the ratio of the average power transmitted from node a to the noise power encountered at the receiver of node b ² as

$$\Gamma_t = \frac{\mathbb{E}\{|x_{a,j}|^2\}}{N_0} = \frac{1}{N_0}. \quad (8)$$

Hence, we have

$$\begin{aligned} \Gamma_r &= \Gamma_t G_{ab} \\ \gamma_r &= \gamma_t + g_{ab} \text{ [dB]} \end{aligned} \quad (9)$$

where $\gamma_r = 10 \log_{10}(\Gamma_r)$, $\gamma_t = 10 \log_{10}(\Gamma_t)$, and the geometrical gain in decibels is given by $g_{ab} = 10 \log_{10}(G_{ab})$. Hence, we can achieve the desired receive SNR by simply changing the transmit power (which governs γ_t) or by selecting an RN at an appropriate geographical location (which defines g_{ab}). In other words, the channel state information (CSI) is not required

²This definition is in line with [6] and [30], but it is unconventional, because it relates the transmit power to the receiver noise measured at two distinct locations.

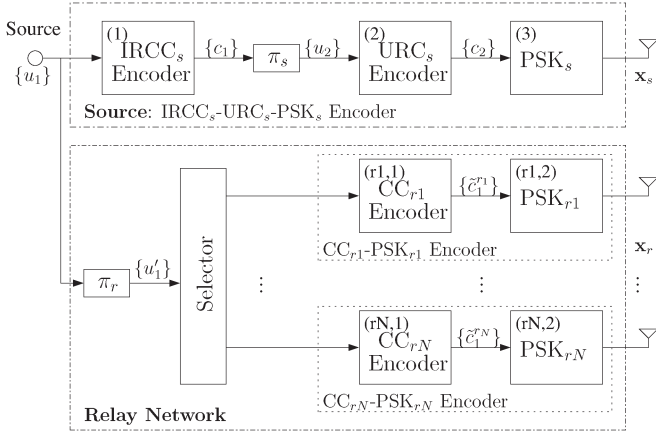


Fig. 2. Schematic of the equivalent DIRCC encoder when perfect decoding is achieved at RNs. The bit-based interleavers at the SN and the relay network are denoted as π_s and π_r , respectively.

for computing the average receive SNR at each transmission symbol period.

A. Encoder Structure

We consider employing a powerful serial concatenation of an IRCC and a recursive unity-rate code (URC) [31] at the SN. The serially concatenated IRCC and URC scheme has been beneficially used in various near-capacity designs [25]–[27], [32]–[34]. More specifically, URCs were proposed by Divsalar *et al.* [31] for the sake of extending the overall system’s impulse response to an infinite duration, which efficiently spreads the extrinsic information between the decoders for improving the achievable iterative detection gain. At the SN, we employ an IRCC as the outer code (IRCC_s), a recursive unity-rate code (URC) as the inner code (URC_s), and a simple phase-shift keying (PSK) modulator (PSK_s), as shown in Fig. 2, to approach the capacity of the source-to-relay channels.

We invoke the DAF protocol for all RNs. At each RN, the IRCC_s-URC_s-PSK_s decoder, shown in the upper part of Fig. 3, is used for generating the estimate of the information bit sequence $\{u_1\}$, before it is fed to the interleaver π_r in Fig. 2. In the absence of decoding errors at the RNs, the input sequence (or the decoded bit sequence) of the “distributed” relay network would be exactly the same as that of the SN. Hence, the equivalent DIRCC encoder structure can be simplified, as seen in the schematic in Fig. 2. The “selector” block shown in Fig. 2 assigns the IRCC code-component weights based on an EXIT-curve-matching procedure to be detailed in Section III-B. We will demonstrate that near-error-free decoding is achieved at channel SNRs close to the SNR limit at the capacity of the relay channels. The IRCC weight of the specific IRCC_s at the SN is also designed based on an EXIT-curve-matching procedure to be detailed in Section III-B for approaching the capacity of the source-to-relay channels. The k th RN would produce an encoded sequence of $\tilde{c}_1^{r,k} = [\tilde{c}_{1,1}^{r,k} \tilde{c}_{1,2}^{r,k} \dots \tilde{c}_{1,j}^{r,k} \dots]$, which is part of the virtual IRCC-encoded sequence $\tilde{c}_1 = [\tilde{c}_1^{r,1} \tilde{c}_1^{r,2} \dots \tilde{c}_1^{r,k} \dots]$. Sequence \tilde{c}_1 is mapped onto the PSK symbol sequence \mathbf{x}_r for transmission to the DN during the second transmission phase T_2 .

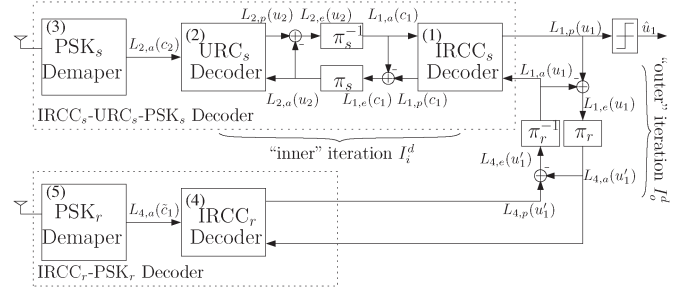


Fig. 3. Schematic of the DIRCC decoder at the DN.

B. Decoder Structure

The equivalent DIRCC decoder at the DN is shown in Fig. 3, where the upper IRCC_s-URC_s-PSK_s decoder corresponds to the upper encoder in Fig. 2, whereas the lower IRCC_r-PSK_s decoder corresponds to the lower encoder in Fig. 2. Iterative decoding is used both within the IRCC_s-URC_s-PSK_s decoder as well as between the upper and lower decoders, as shown in Fig. 3.

The maximum *a posteriori* probability (MAP) algorithm [25] is invoked by each decoder. Note that the *extrinsic* log-likelihood ratio (LLR) of a bit c is given by the subtraction of the *a priori* LLR from the *a posteriori* LLR [25] as $L_{i,e}(c) = L_{i,p}(c) - L_{i,a}(c)$, where subscript i is used for identifying the specific detection block, which is labeled with (i) on the top-left corner of its block diagram, as shown in Fig. 3. More specifically, each of the *a priori* LLR $L_{2,a}(c_2)$ corresponding to the URC_s-encoded bit c_2 is produced by the PSK demapper, as shown in Fig. 3. The *inner* decoding iteration is performed between the URC_s decoder and the IRCC_s decoder, based on the *a priori* or *extrinsic* LLRs of the IRCC_s-encoded bits $\{c_1\}$ or its π_s -interleaved version, namely, the input bits of URC_s $\{u_2\}$. By contrast, the *outer* iteration between the upper and lower decoders is based on the LLRs of the source bits $\{u_1\}$ and on its π_r -interleaved version $\{u'_1\}$. Note that only one IRCC_r decoder is needed for decoding all transmitted symbols from the K -RN-assisted relay network. Iterative detection between the upper and lower decoder blocks makes information exchange possible between the two detection phases, namely, T_1 and T_2 , for the sake of approaching the overall relay channel capacity.

III. NEAR-CAPACITY SYSTEM DESIGN

Let us now consider the relay channel capacity and the design of our near-capacity DIRCC.

A. Relay Channel Capacity

The two-hop half-duplex relay channel capacity can be calculated by modifying the full-duplex relay channel capacity computation derived in [35]. More specifically, the upper bound C^U and lower bound C^L of our half-duplex relay channel capacity can be computed by considering the capacity of the channel between the SN, RNs, and DN as follows:

$$C^U = \min \{ \lambda C_{(s \rightarrow r, d)}, \lambda C_{(s \rightarrow d)} + (1 - \lambda) C_{(r \rightarrow d)} \} \quad (10)$$

$$C^L = \min \{ \lambda C_{(s \rightarrow r)}, \lambda C_{(s \rightarrow d)} + (1 - \lambda) C_{(r \rightarrow d)} \} \quad (11)$$

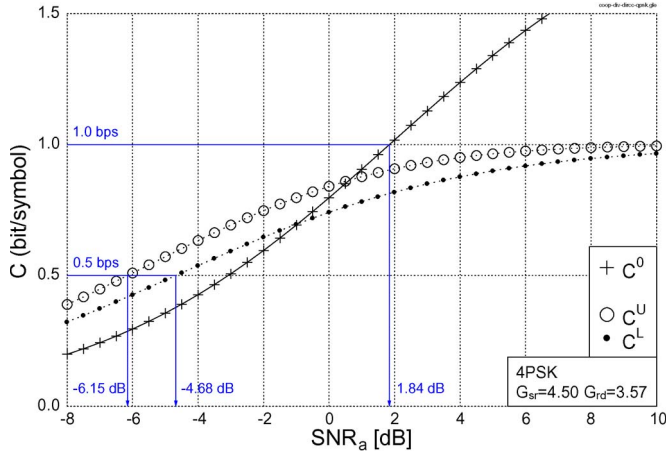


Fig. 4. 4PSK-based DCMC capacity curves of the relay channel.

where $C_{(a \rightarrow b, c)}$ is the capacity of the channel between the transmitter at node a and the receivers at both node b and node c . Similarly, $C_{(a \rightarrow b)}$ is the capacity of the channel between the transmitter at node a and the receiver at node b . Note that the capacity term $C_{(a \rightarrow b, c)}$ or $C_{(a \rightarrow b)}$ can be either continuous-input-continuous-output memoryless channel capacity or modulation-dependent discrete-input-continuous-output memoryless channel (DCMC) capacity [2], [36]. The DCMC capacity is also referred to as the constrained information rate. The ratio of the first transmission period to the total transmission period is given by $\lambda = N_s / (N_s + N_r)$. In this contribution, we consider $N_s = N_r$, where N_r is given by (6). This gives $\lambda = 1/2$. Note furthermore that the term $C_{(s \rightarrow r, d)}$ considered in the upper bound of (10) assumes that the RN and the DN are capable of perfectly sharing their received signals for joint detection, which is not possible when the RN and the DN are not colocated or linked. By contrast, the lower bound is a more practical measure, since it treats the signals received at the RN and the DN independently.

The upper and lower bounds of the relay channel capacity curves, which are based on 4PSK DCMC, are shown in Fig. 4 for $\lambda = 0.5$, $G_{sr_k} = 4.50$, and $G_{rd} = 3.57$, where SNR_a is the average transmit SNR defined in (8). The geometrical gains G_{sr_k} and G_{rd} are chosen based on the relay selection mechanism explained in Section III-C. The 4PSK-based DCMC capacity C^0 of the direct link is also shown in Fig. 4 for comparison. As seen in Fig. 4, a half-rate 4PSK-based scheme has an SNR limit of 1.84 dB, where an error-free throughput of 1 bit per symbol (BPS) is achieved. By contrast, the relay channel capacity of the half-duplex 4PSK-based scheme has SNR limits of -4.68 and -6.15 dB for its lower and upper bounds, respectively, when aiming for a throughput of 0.5 BPS. Note that the capacity of the relay channel (both C^U and C^L) is higher than that of the direct link (C^0), when $SNR_a \leq -1$ dB due to the reduced path loss introduced by the RNs. However, the asymptotic capacity of the relay channel is lower than that of the direct link due to the half-duplex constraint.

B. Irregular Code Design

According to the so-called area property of the EXIT chart [23], [24], it can be shown that the area under the normal-

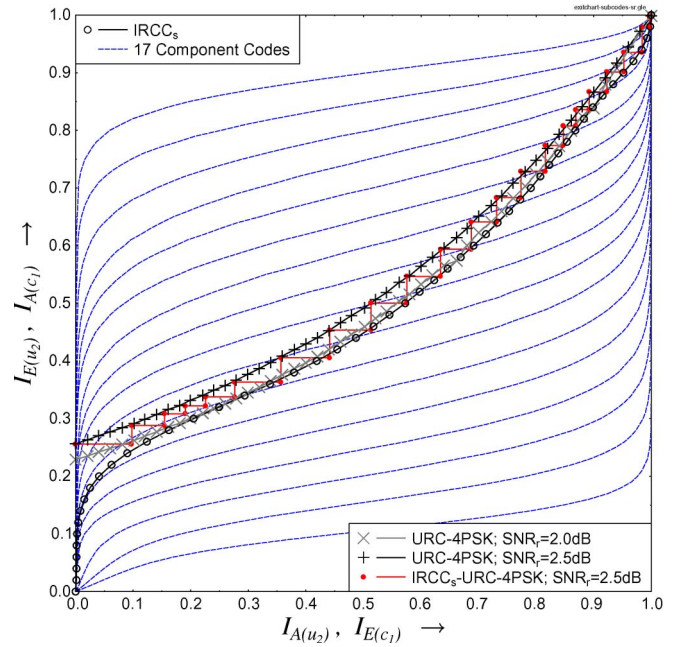


Fig. 5. EXIT chart of the IRCC_s-URC_s-4PSK decoder at each RN.

ized EXIT curve of an inner decoder/demapper is related to the achievable DCMC capacity. On the other hand, the area under the inverted EXIT curve of an outer decoder is equal to its coding rate R . Based on these EXIT chart properties, a near-capacity concatenated coding scheme can be designed by matching the corresponding inner and outer decoder EXIT curves, so that a narrow but marginally open EXIT chart tunnel exists between them all the way to the $(x, y) = (1, y)$ point, where $x = I_{E(u_2)} = I_{A(c_1)}$, and $y = I_{A(u_2)} = I_{E(c_1)} \in \{0, 1\}$ for the EXIT chart in Fig. 5. Note that $I_{A(b)}$ and $I_{E(b)}$ denote the *a priori* and *extrinsic* information, respectively, of $b \in \{c_1, u_2\}$, which is either the outer encoder's output bit c_1 or the inner encoder's input bit u_2 . The design of the IRCC is normally carried out offline, particularly when communicating over fast Rayleigh fading channels. However, when transmitting over slow-fading channels, it may be more beneficial to design the IRCC in real time, by adapting the IRCC coefficients to the prevalent channel conditions. For simplicity, we only consider transmissions over fast Rayleigh fading channels in this paper.

1) *Code Design for SN:* For the IRCC_s design at the SN, we consider an IRCC that consists of $P = 17$ memory-4 convolutional codes (CCs) given in [23] and [24]. A total encoded sequence length of $N_c = 120\,000$ bits and an effective coding rate of $R = 0.5$ are considered. The p th subcode has a coding rate of R_p , and it encodes a fraction of $\alpha_p R_p N_c$ information bits to $\alpha_p N_c$ encoded bits. More specifically, α_p is the p th IRCC weighting coefficient satisfying the following constraints [23], [24]:

$$\sum_{p=1}^P \alpha_p = 1, \quad R = \sum_{p=1}^P \alpha_p R_p, \quad \alpha_p \in [0, 1] \quad \forall p \quad (12)$$

which can be conveniently represented in the following matrix form:

$$\begin{bmatrix} 1 & 1 & \dots & 1 \\ R_1 & R_2 & \dots & R_P \end{bmatrix} [\alpha_1 \ \alpha_2 \ \dots \ \alpha_P]^T = \begin{bmatrix} 1 \\ R \end{bmatrix} \quad \mathbf{C} \boldsymbol{\alpha} = \mathbf{d}. \quad (13)$$

The EXIT function of the IRCC is given by

$$I_{E(c_1)} = T_{c_1} [I_{A(c_1)}] = \sum_{p=1}^P \alpha_p T_{c_1,p} [I_{A(c_1)}] \quad (14)$$

where $T_{c_1,p} [I_{A(c_1)}] = I_{E(c_1),p}$ is the EXIT function of the p th subcode. More explicitly, the inverted EXIT curves of the $P = 17$ subcodes having different coding rates ranging from 0.1 to 0.9 are shown in Fig. 5. The vertical difference between the inner and outer code's EXIT curves at a given $I_{A(u_2)}$ value is given by

$$e(I_{A(u_2)}) = I_{E(u_2)} - I_{A(c_1)} \quad (15)$$

$$= T_{u_2} [I_{A(u_2)}, C_*] - \sum_{p=1}^P \alpha_p T_{c_1,p}^{-1} (I_{E(c_1)}) \quad (16)$$

where the EXIT function of the inner decoder depends on both $I_{A(u_2)}$ and on the DCMC capacity C_* . Fig. 5 shows that it is possible to design an IRCC_s for the SN to have an EXIT curve that matches the EXIT curve of the URC_s-4PSK inner encoder at a receive SNR of 2 dB. Here, c_1 is the coded bit of the IRCC_s outer encoder, and u_2 denotes the interleaved version of c_1 , which is fed to the URC_s-4PSK inner encoder. We found that IRCC_s only requires seven out of the 17 available component codes, i.e., there are only seven nonzero IRCC weights. The corresponding IRCC weight vector is given by

$$\tilde{\boldsymbol{\alpha}}_s = [0.2356z_{0.30}^5 \ 0.2052z_{0.35}^6 \ 0.0859z_{0.40}^7 \ 0.2114z_{0.55}^{10} \ 0.1284z_{0.70}^{13} \ 0.0630z_{0.85}^{16} \ 0.0705z_{0.90}^{17}] \quad (17)$$

where the exponent and the subscript of the dummy variable z denote the component code index p and its coding rate R_p , respectively, whereas the p th IRCC weight α_p is the value in front of $z_{R_p}^p$.

According to the capacity curve C^0 in Fig. 4, the corresponding transmit SNR at a capacity of 1 BPS is 1.84 dB. Hence, the IRCC_s-URC_s-4PSK scheme is capable of operating within $(2 - 1.84) = 0.16$ dB from the SNR limit of the source-to-relay channel. However, the narrow gap between the two EXIT curves shown in Fig. 5 would require an impractically high number of decoding iterations at the RN. Hence, we aim for attaining a receive SNR of $\gamma_x^{sr} = 2.5$ dB instead of 2 dB at the RN to achieve a wider gap between these EXIT curves for attaining lower decoding complexity. Note that these two EXIT curves are generated semianalytically to predict the actual performance of the IRCC_s-URC_s-4PSK scheme. A Monte-Carlo-simulation-based staircase-shaped decoding trajectory of the IRCC_s-URC_s-4PSK scheme at $\gamma_x^{sr} = 2.5$ dB is shown in Fig. 5 to satisfy the EXIT chart prediction, where it

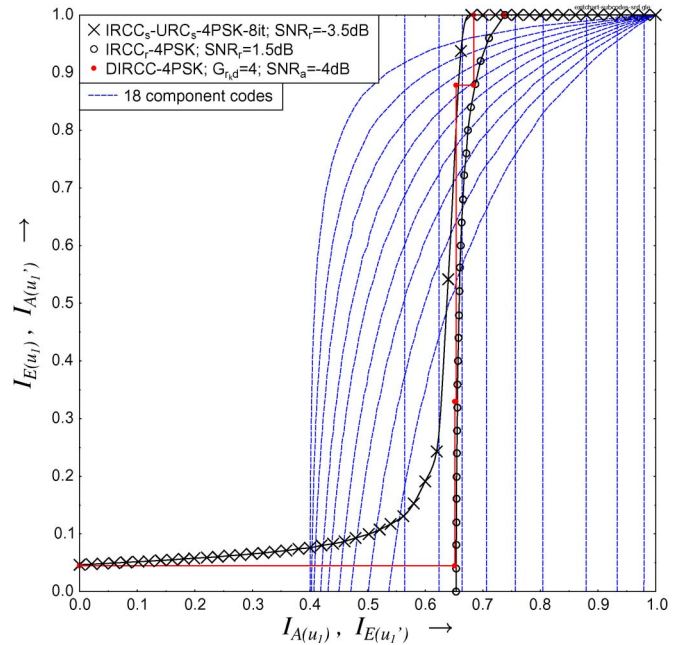


Fig. 6. EXIT chart of the DIRCC-4PSK decoder at the DN.

traverses within the gap between the two EXIT curves up to the top-right corner.

2) *Code Design for RNs*: The design of DIRCC involves the IRCC_s-URC_s-4PSK scheme as the upper decoder and the IRCC_r-4PSK scheme as the lower decoder in Fig. 3. Once the IRCC_s has been designed for the source-to-relay channel, the next task is to design the IRCC_r. However, the design of IRCC_r for the relay network is more challenging, because the EXIT curves of both the upper and lower decoders are SNR dependent. The EXIT curve of the IRCC_s-URC_s-4PSK upper decoder at the DN is shown in Fig. 6 when the receive SNR is $\gamma_x^{sd} = -3.5$ dB,³ where eight inner decoding iterations⁴ are considered. An IRCC_r is designed to have an EXIT curve that can closely match the EXIT curve of the IRCC_s-URC_s-4PSK decoder.

We found that the memory-4 17-component IRCC in [23] fails to ensure a good match to the steep IRCC_s-URC_s-4PSK EXIT curve shown in Fig. 6. On the other hand, a simple repetition code (RC) would give a vertical EXIT curve that can match the vertical part of the IRCC_s-URC_s-4PSK EXIT curve. Hence, we have created nine RCs having coding rates ranging from 0.1 to 0.5 with a step size of 0.05. Their EXIT curves are shown by the nine vertical dashed lines in Fig. 6, where the rightmost vertical curve has the lowest coding rate of 0.1 and the leftmost vertical curve has the highest coding rate of 0.5. To match the gradually sloping part of the IRCC_s-URC_s-4PSK EXIT curve, we have created nine further component CCs, having coding rates ranging from 0.5 to 0.9 with a step size of 0.05. The mother code of these CCs is a half-rate unit-memory CC having a generator polynomial of [2 1] in octal

³The rationale of considering $\gamma_x^{sd} = -3.5$ dB is explained in Section III-C.

⁴It was found that having more than eight inner iterations will only marginally increase the area under the EXIT curve of the IRCC_s-URC_s-4PSK decoder.

format. The same puncturing patterns of the 17-component IRCC in [23] are used for creating CCs having coding rates higher than 0.5. The corresponding nine EXIT curves are shown by the gradually sloping EXIT curves in Fig. 6, where the rightmost curve has the lowest coding rate of 0.5, and the leftmost curve has the highest coding rate of 0.9. Based on these 18 newly created component codes, an IRCC_r-4PSK lower encoder was designed. Its EXIT curve is also shown in Fig. 6. The corresponding IRCC weight vector is given by

$$\tilde{\alpha}_r = [0.60z_{0.60}^8 \ 0.30z_{0.50}^9 \ 0.10z_{0.85}^{17}] \quad (18)$$

where the eighth and ninth subcodes are from the RC family, while the 17th subcode is from the unit-memory CC family. Hence, we only need three RNs for our system with only a low-complexity RC or a unit-memory CC needed as the RN encoder.

The proposed design was based on a conventional EXIT chart, where a sufficiently long interleaver is required for the Monte Carlo simulation to warrant a good match between the EXIT chart prediction and the actual simulation. We found that an interleaver length of 120 000 bits is sufficient for the interleaver between the IRCC_s and URC_s encoders. The encoded bit sequence can be stored in a buffer for transmission over several frame periods, if the transmission frame duration is shorter than the encoded sequence length. However, if the system requires a short interleaver, we should redesign the proposed scheme based on EXIT band charts [37], while using the same design principle.

C. Power Allocation and Relay Selection

The receive SNR required at the RN during T_1 is given by $\gamma_x^{sr} = 2.5$ dB, as shown in Fig. 5, whereas the receive SNR needed at the DN during T_2 is given by $\gamma_x^{rd} = 1.5$ dB, as shown in Fig. 6. The idea of the design is to simultaneously achieve these two receive SNRs at the RN and the DN, respectively, to achieve a bit error rate (BER) lower than 10^{-6} at all RNs and DN at the same time. When this is achieved, there will be minimal error propagation from the DAF-based RNs. Since the receive SNR depends on the geometrical gain as shown in (9), we may achieve the required receive SNR with the aid of relay selection, which determines the geometrical gains based on the location of the RN according to (2) and (5). When communicating over fast Rayleigh fading channels, RN selection can be predetermined based on the RN locations, without the need for CSI knowledge at each transmission symbol period, because the average power of the fast Rayleigh channel coefficients is unity. By contrast, RN selection is a dynamic process, depending on the instantaneous channel variations when transmitting over slow-fading channels. We consider fast Rayleigh fading channels in this contribution. Since the receive SNR also depends on the transmit SNR according to (9), we may calculate the minimum required transmission power and then appropriately share it between the SN and RNs. CSI knowledge is not required⁵ for the power allocation mechanism either when transmitting

over fast Rayleigh fading channels. We assumed that a base station or a central node carries out the RN selection and/or power allocation, followed by broadcasting this information to the participating nodes.

1) *Power Allocation*: When the number of available RNs is limited and their locations are fixed, power allocation/control can be used for improving power efficiency. Assuming for simplicity that all RNs are located midway between the SN and the DN, we have geometrical gains of $G_{sr_k} = G_{r_kd} = 4$. To achieve $\gamma_x^{sr} = 2.5$ dB at the RN, the corresponding transmit SNR at the SN is given by $\gamma_t^s = 2.5 - 10 \log_{10}(G_{sr_k}) = -3.5$ dB according to (9). Since we have $G_{sd} = 1$, the corresponding receive SNR at the DN during T_1 is given by $\gamma_x^{sd} = \gamma_t^s = -3.5$ dB. The EXIT curve of the IRCC_s-URC_s-4PSK scheme at $\gamma_x^{sd} = \gamma_t^s = -3.5$ dB is shown in Fig. 6. Furthermore, the required receive SNR at the DN during T_2 is given by $\gamma_x^{rd} = 1.5$ dB, and the corresponding transmit SNR at the RN is given by $\gamma_t^r = 1.5 - 10 \log_{10}(G_{r_kd}) = -4.5$ dB when $G_{r_kd} = 4$. Hence, the transmit power at the SN has to be $\gamma_t^s - \gamma_t^r = 1$ dB higher than that of the RN, to simultaneously achieve an infinitesimally low BER at all RNs and the DN. The average transmit SNR of the power-allocation-based DIRCC scheme is given by

$$\tilde{\gamma}_t = 10 \log_{10} \left(\lambda 10^{\gamma_t^s/10} + (1 - \lambda) 10^{\gamma_t^r/10} \right) \quad (19)$$

which is equal to $\tilde{\gamma}_t = -4$ dB for $\gamma_t^s = -3.5$ dB and $\gamma_t^r = -4.5$ dB, where $\lambda = 0.5$, as discussed in Section III-A. The simulation-based decoding trajectory of the DIRCC-4PSK scheme is shown to verify the EXIT chart predictions in Fig. 6, when $\tilde{\gamma}_t = -4$ dB.

2) *Relay Selection*: Alternatively, if the transmit power of the SN and of all the RNs is fixed to a constant value of $\gamma_t^r = \gamma_t^s$, we may select RNs at appropriate geographical locations for achieving different G_{sr_k} and G_{r_kd} values, to simultaneously maintain $\gamma_x^{sr} = 2.5$ dB and $\gamma_x^{rd} = 1.5$ dB. Assuming that all RNs are relatively close to each other and are located in the direct SN-to-DN path, where we have $d_{sd} = d_{sr_k} + d_{r_kd}$, it can be shown that the geometrical gains are related to each other as follows:

$$G_{r_kd} = \left(\frac{1}{1 - 1/\sqrt{G_{sr_k}}} \right)^2. \quad (20)$$

Furthermore, since we have $\gamma_t^s = \gamma_t^r$, it can be shown based on (9) that

$$\frac{G_{r_kd}}{G_{sr_k}} = 10^{(\gamma_x^{rd} - \gamma_x^{sr})/10} \quad (21)$$

where we have $\gamma_x^{rd} - \gamma_x^{sr} = 1.5 - 2.5 = -1$ dB in our example. Based on (20) and (21), we have the following relationship:

$$G_{sr_k} = \left(1 + 10^{-(\gamma_x^{rd} - \gamma_x^{sr})/20} \right)^2 \quad (22)$$

which gives $G_{sr_k} = 4.50$ for our case, and from (20), we have $G_{r_kd} = 3.58$. Once G_{sr_k} and G_{r_kd} are identified, we may find the corresponding relay distances from (2) and (5), which are given by $d_{sr_k} = 0.47d_{sd}$ and $d_{r_kd} = 0.53d_{sd}$, respectively.

⁵CSI knowledge is only needed at the receiver for decoding purposes, where each RN only has to know the CSI between the SN and itself, whereas the DN only has to know the CSI between the corresponding RNs/SN and itself.

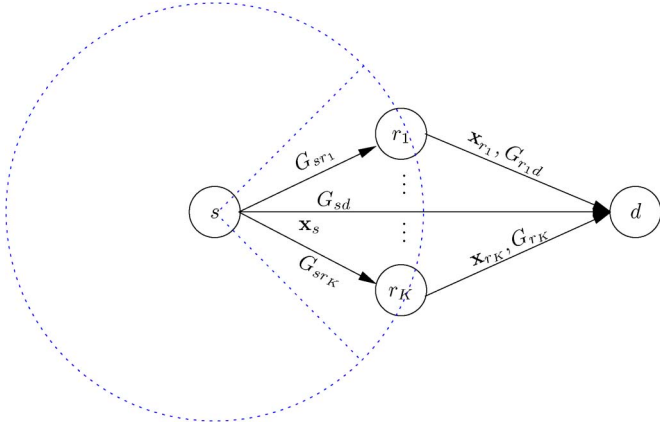


Fig. 7. Relay selection schematic for the DIRCC scheme.

The average transmit SNR of the relay-selection-based DIRCC scheme is given by

$$\tilde{\gamma}_t = \gamma_t^r = \gamma_t^s = \gamma_x^{sr} - 10 \log_{10}(G_{sr_k}) \quad (23)$$

where we have $\tilde{\gamma}_t = -4$ dB for our example, which is the same value as that of the power-allocation-based scenario.

3) *Joint Power Allocation and Relay Selection:* In the non-ideal case, when the RNs are not located in the direct SN-to-DN path, we have to invoke the following approach, which employs both relay selection and power allocation for minimizing the overall transmission power.

- 1) Calculate the minimum required receive SNR at the RN during T_1 , $\gamma_{x,\min}^{sr}$, and at the DN during T_2 , $\gamma_{x,\min}^{rd}$, based on the EXIT chart analysis described in Section III-B.
- 2) For a given SN transmit SNR γ_t^s , select those specific RNs that can satisfy the SNR requirement of $\gamma_x^{sr} \geq \gamma_{x,\min}^{sr}$ for ensuring a low BER at each RN. Normally, the geographical range is within a circle having the SN at its center, as shown in Fig. 7. More explicitly, we have $d_{sr_k} \leq \sqrt{G_{sr_k} d_{sd}}$, where G_{sr_k} is given by (22).
- 3) From the appropriately chosen set of RNs, select K RNs that have high-SNR RN-to-DN links to form a virtual IRCC that consists of K component codes. Normally, the geographical range is within the quarter of the circle facing the DN, as shown in Fig. 7.
- 4) If the number of available RNs ($K_r \geq 1$) is less than the number of IRCC _{r} component codes, i.e., $K_r < K$, some of the RNs will have to perform several IRCC component encoding operations. Again, the number of symbols transmitted by each RN is different.
- 5) Each RN takes turns in transmitting, while using the minimum power that can satisfy the following RN transmit SNR: $\gamma_{t,\min}^r = \gamma_{x,\min}^{rd} - g_{r_k d}$ according to (9). When communicating over slow- or shadow-fading channels, (9) would have to take into consideration the instantaneous channel gain $h_{r_k d}$. Hence, the RN transmission power may change with its location or with time, where the average transmit SNR of the DIRCC scheme is given by (19).

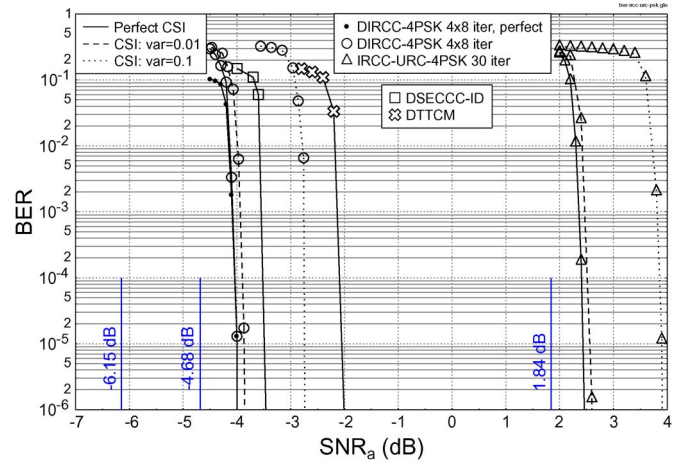


Fig. 8. BER-versus- SNR_a performance of the proposed DIRCC-4PSK scheme in comparison with perfect DIRCC-4PSK, IRCC-URC-4PSK, DSECCC-ID, and DTTCM schemes, when communicating over fast Rayleigh fading channels using a frame length of 60 000 4PSK symbols.

Furthermore, relay selection should also take into account the battery life of each RN, if this information is available. More specifically, an RN with insufficient battery life should not be chosen as part of the virtual IRCC. Since each IRCC component encoder produces a different number of modulated symbols, RNs having a longer battery life should be assigned to the specific component code that produces the longest coded/modulated sequence, i.e., the highest L_k value given in (6), which is normally related to a higher IRCC weight or a lower coding rate. In the following simulation study, we only consider the ideal case where all RNs have sufficient battery life for the whole transmission process.

IV. RESULTS AND DISCUSSIONS

Let us first investigate the performance of the proposed scheme, when perfect CSI is available at each receiver. The BER-versus-average-transmit-SNR performance of the proposed DIRCC-4PSK scheme is compared with both that of perfect⁶ DIRCC-4PSK and that of the noncooperative IRCC-URC-4PSK schemes in Fig. 8, based on the simulation parameters of Table I. The noncooperative IRCC-URC-4PSK scheme has 30 decoding iterations at the DN. It operates approximately 0.65 dB away from its channel capacity at $\text{BER} = 10^{-6}$. Both DIRCC-4PSK schemes have eight inner iterations and four outer iterations at the DN. Relay selection was considered in the simulations, and all three RNs considered are assumed to be located in the direct SN-to-DN path. Hence, we have $G_{sr_k} = 4.50$ and $G_{r_k d} = 3.57$ for all three RNs according to (22) and (20), respectively, with the aid of the relay selection mechanism detailed in Section III-C2. As seen in Fig. 8, the proposed DIRCC-4PSK scheme has negligible performance difference to that of the perfect DIRCC-4PSK scheme for

⁶The perfect DIRCC-4PSK scheme assumes that there are no decoding errors at each RN, whereas the actual DIRCC-4PSK scheme considers a realistic SN-to-RN transmission and actual decoding with potential decoding errors at each RN.

TABLE I
SIMULATION PARAMETERS

Modulation	4PSK
Number of modulated symbols/frame	60,000
Interleaver	Random and bit-based
IRCC weights, $\tilde{\alpha}_s$	See (17)
DIRCC weights, $\tilde{\alpha}_r$	See (18)
Coding rate of IRCC	0.5
Coding rate of DIRCC	0.5
Number of IRCC-URC-4PSK iterations	30
Number of DIRCC inner iterations	8
Number of DIRCC outer iterations	4
Decoding algorithm	Approximated Log-MAP [25]
Channel type	Fast Rayleigh fading
SN-to-RN geometrical gain, G_{srk}	4.50 (6.53 dB)
RN-to-DN geometrical gain, G_{rkd}	3.57 (5.53 dB)

BER $< 10^{-2}$. This is due to the efficient relay selection mechanism. The proposed scheme is also capable of operating within 0.68 dB from the lower bound of the channel capacity. This near-capacity performance is achieved with the advent of an effective system design, as detailed in Section III, with the aid of powerful iterative decoding at all of the RNs and at the DN.

Let us now investigate the performance of the proposed DIRCC scheme in comparison to both the distributed TTCM (DTTCM) [13] and the distributed self-concatenated convolutional coding relying on iterative detection (SECCC-ID) [18] schemes, when perfect CSI is assumed. All schemes employ a frame length of 60 000 4PSK symbols for transmission over fast Rayleigh fading channels. The throughput of the 4PSK-based SECCC-ID scheme is 0.5 BPS, which is exactly identical to that of the proposed 4PSK-based DIRCC scheme. However, the throughput of the 4PSK-based DTTCM⁷ scheme is 0.667 BPS, because it only transmits parity bits from the RN to the DN. As seen in Fig. 8, the DIRCC scheme outperforms the DSECCC-ID and DTTCM schemes by approximately 0.5 and 2.0 dB,⁸ respectively, at a BER of 10^{-6} . We found that the proposed DIRCC scheme performs the closest to the relay channel's capacity, when aiming for a throughput of 0.5 BPS, compared with existing DAF-based distributed coding schemes found in the literature, when communicating over fast Rayleigh fading channels using a single antenna at each node.

When the CSI is not perfectly known at the receiver, our coherently detected scheme would suffer from some performance erosion. To investigate the robustness of our DIRCC scheme to imperfect CSI, we model the channel estimation errors by a Gaussian process superimposed on each channel coefficient at the receiver, where the noise variances of 0.01 and 0.1 are used. The corresponding performance curves of DIRCC-4PSK and IRCC-URC-4PSK are shown in Fig. 8, where a CSI estimation error with a variance of 0.01 would only cause a marginal loss of approximately 0.2 dB at a BER of 10^{-6} . By contrast, an error with a variance of 0.1 would impose a more

⁷The original DTTCM scheme in [13] employed 2/3-rate TTCM-8PSK at the SN and uncoded-4PSK at the RN. The DTTCM scheme considered here uses 1/2-rate TTCM-4PSK at the SN and uncoded-4PSK at the RN to make its throughput as close as possible to the proposed DIRCC scheme for a fair comparison.

⁸In terms of SNR per information bit, the gain of DIRCC over DTTCM is given by $2.0 \text{ dB} + 10 \log_{10}(0.667) - 10 \log_{10}(0.50) = 0.76 \text{ dB}$.

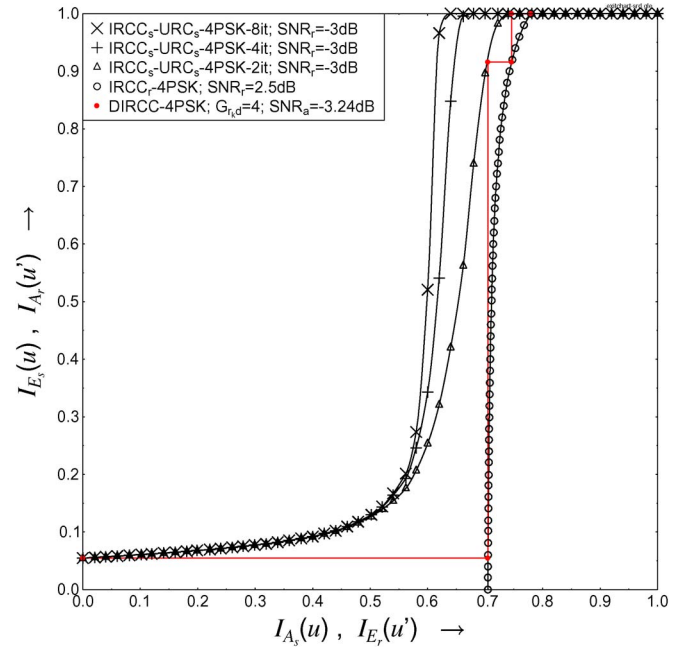


Fig. 9. EXIT chart of the low-complexity DIRCC-4PSK decoder at the DN.

substantial but still moderate SNR loss of approximately 1.3 dB on the DIRCC scheme. This loss is lower than the 3-dB loss incurred by conventional noncoherent schemes [38]. Hence, our DIRCC scheme may be deemed robust to CSI estimation errors. In both imperfect-CSI cases, we ensured that appropriate RN selection (or power allocation) was invoked for the DIRCC scheme for ensuring that the decoders at both the RNs and DN are capable of simultaneously achieving a low BER, according to the mechanism described in Section III-C.

However, the decoding complexity at the DN is rather high due to the high number of inner iterations between the memory-4-based IRCC_s decoder and the unit-memory URC_s decoder. Let us denote the number of decoding trellis states per iteration of the upper IRCC_s-URC_s-4PSK decoder as $I_U = 2^4 + 2^1 = 18$ states and that of the unit-memory CC (or RC)-based lower IRCC_r-4PSK decoder as $I_L = 2^1 = 2$ states. The total number of trellis states invoked for the DIRCC-4PSK scheme would be $I = 4 \times (8I_U + I_L) = 584$ states. We found that the decoding complexity at the DN can be significantly reduced if a slightly higher value than the minimum transmit power is used. More explicitly, let us consider the scheme shown in Fig. 9, where $G_{rkd} = G_{srk} = 4$. The transmit SNR at the SN and the RN is $3 - 10 \log_{10}(4) = -3$ dB and $2.5 - 10 \log_{10}(4) = -3.5$ dB, respectively. Hence, the corresponding average transmit SNR is given by -3.24 dB according to (19). As seen in Fig. 9, two inner iterations and three outer iterations are sufficient for achieving an infinitesimally low BER at this setting. In other words, when operating at $-3.24 - (-4) = 0.76$ dB higher average transmit SNR, the DIRCC-4PSK decoder would only incur $I = 3 \times (2I_U + I_L) = 114$ trellis states, which is only 19.5% of the original decoding complexity. A higher reduction of the decoding complexity can be achieved, when operating further away from the SNR limit of the channel capacity. Furthermore, based on the EXIT chart in Fig. 5, we found that

the average number of decoding iterations at each RN is given by 97, 25, or 17 when the receive SNRs are given by 2, 2.5, or 3 dB, respectively. The receive SNR at each RN is given by 2.5 or 3 dB, when the average transmit SNR is given by -4 or -3.24 dB, respectively. Hence, the total number of decoding states at each RN is also reduced by 32%, i.e., from $25I_U = 450$ to $17I_U = 306$ states, when a 0.76-dB higher average transmit SNR is employed. In summary, the proposed DIRCC scheme can be designed according to the target transmit power, where a high-complexity scheme is invoked when aiming for approaching the channel capacity, whereas a lower complexity scheme can be designed when operating slightly further away from the SNR limit of the channel capacity.

V. CONCLUSION

A near-capacity DIRCC scheme has been proposed for assisting DAF-based cooperative communications. The potential decoding errors at each RN may be avoided by the proposed relay selection mechanism, whereas the transmission power of the DIRCC scheme can be reduced by invoking the proposed power allocation method. Furthermore, a low-complexity encoder was used by each RN for yielding a variable-length coded/modulated symbol sequence. The semianalytical EXIT-chart-based performance predictions were verified by simulation results. It was shown that the proposed DIRCC scheme is capable of operating close to the relay channel's capacity, and it outperforms the existing distributed coding schemes operating in a similar simulation environment at a similar throughput. It was also shown that the DIRCC scheme is robust to channel estimation errors at the receiver. The proposed DIRCC scheme can be further developed for supporting communications over shadow-fading channels. It can also be adapted according to the battery life of the RNs. More advanced modulation schemes, including hierarchical modulation and superposition modulation, may also be utilized in the proposed DIRCC scheme.

REFERENCES

- [1] E. Telatar, "Capacity of multi-antenna Gaussian channels," *Eur. Trans. Telecommun.*, vol. 10, no. 6, pp. 585–595, Nov./Dec. 1999.
- [2] S. X. Ng and L. Hanzo, "On the MIMO channel capacity of multi-dimensional signal sets," *IEEE Trans. Veh. Technol.*, vol. 55, no. 2, pp. 528–536, Mar. 2006.
- [3] A. Sendonaris, E. Erkip, and B. Aazhang, "User cooperation diversity Part I: System description," *IEEE Trans. Commun.*, vol. 51, no. 11, pp. 1927–1938, Nov. 2003.
- [4] N. Laneman, D. N. C. Tse, and G. W. Wornell, "Cooperative diversity in wireless networks: Efficient protocols and outage behavior," *IEEE Trans. Inf. Theory*, vol. 50, no. 12, pp. 3062–3080, Dec. 2004.
- [5] Y. Li, "Distributed coding for cooperative wireless networks: An overview and recent advances," *IEEE Commun. Mag.*, vol. 47, no. 8, pp. 71–77, Aug. 2009.
- [6] B. Zhao and M. C. Valenti, "Distributed turbo coded diversity for relay channel," *IEE Electron. Lett.*, vol. 39, no. 10, pp. 786–787, May 2003.
- [7] M. Janani, A. Hedayat, T. Hunter, and A. Nosratinia, "Coded cooperation in wireless communications: Space-time transmission and iterative decoding," *IEEE Trans. Signal Process.*, vol. 52, no. 2, pp. 362–371, Feb. 2004.
- [8] Z. Zhang and T. Duman, "Capacity-approaching turbo coding for half-duplex relaying," *IEEE Trans. Commun.*, vol. 55, no. 10, pp. 1895–1906, Oct. 2007.
- [9] Y. Li, B. Vucetic, and J. Yuan, "Distributed turbo coding with hybrid relaying protocols," in *Proc. IEEE PIMRC*, Cannes, France, Sep. 15–18, 2008.
- [10] A. Chakrabarti, A. Baynast, A. Sabharwal, and B. Aazhang, "Low density parity check codes for the relay channel," *IEEE J. Sel. Areas Commun.*, vol. 25, no. 2, pp. 280–291, Feb. 2007.
- [11] A. Chakrabarti, A. Baynast, A. Sabharwal, and B. Aazhang, "Low density parity check codes over wireless relay channels," *IEEE Trans. Wireless Commun.*, vol. 6, no. 9, pp. 3384–3394, Sep. 2007.
- [12] P. Razaghi and W. Yu, "Bilayer low-density parity-check codes for decode-and-forward in relay channels," *IEEE Trans. Inf. Theory*, vol. 53, no. 10, pp. 3723–3739, Oct. 2007.
- [13] S. X. Ng, Y. Li, and L. Hanzo, "Distributed turbo trellis coded modulation for cooperative communications," in *Proc. IEEE ICC*, Dresden, Germany, Jun. 14–18, 2009, pp. 1–5.
- [14] L. Lampe, R. Schober, and S. Yiu, "Distributed space-time coding for multihop transmission in power line communication networks," *IEEE J. Sel. Areas Commun.*, vol. 24, no. 7, pp. 1389–1400, Jul. 2006.
- [15] Y. Jing and B. Hassibi, "Distributed space-time coding in wireless relay networks," *IEEE Trans. Wireless Commun.*, vol. 5, no. 12, pp. 3524–3536, Dec. 2006.
- [16] J. Yuan, Z. Chen, Y. Li, and L. Chu, "Distributed space-time trellis codes for a cooperative system," *IEEE Trans. Wireless Commun.*, vol. 8, no. 10, pp. 4897–4905, Oct. 2009.
- [17] L. Kong, S. X. Ng, R. G. Maunder, and L. Hanzo, "Maximum-throughput irregular distributed space-time code for near-capacity cooperative communications," *IEEE Trans. Veh. Technol.*, vol. 59, no. 3, pp. 1511–1517, Mar. 2010.
- [18] M. F. U. Butt, R. A. Riaz, S. X. Ng, and L. Hanzo, "Distributed self-concatenated coding for cooperative communication," *IEEE Trans. Veh. Technol.*, vol. 59, no. 6, pp. 3097–3104, Jul. 2010.
- [19] M. Shirvanimoghadam, Y. Li, and B. Vucetic, "Distributed raptor coding for erasure channels: Partially and fully coded cooperation," *IEEE Trans. Commun.*, vol. 61, no. 9, pp. 3576–3589, Jul. 2013.
- [20] Y. Li, M. S. Rahman, S. X. Ng, and B. Vucetic, "Distributed soft coding with a soft input soft output (SISO) relay encoder in parallel relay channels," *IEEE Trans. Commun.*, vol. 61, no. 9, pp. 3660–3672, Sep. 2013.
- [21] A. Bletsas, A. Khisti, D. P. Reed, and A. Lippman, "A simple cooperative diversity method based on network path selection," *IEEE J. Sel. Areas Commun.*, vol. 24, no. 3, pp. 659–672, Mar. 2006.
- [22] M. Ju and I.-M. Kim, "Relay selection with ANC and TDBC protocols in bidirectional relay networks," *IEEE Trans. Commun.*, vol. 58, no. 12, pp. 3500–3511, Dec. 2010.
- [23] M. Tüchler and J. Hagenauer, "EXIT charts of irregular codes," in *Proc. Conf. Inf. Sci. Syst.*, Mar. 20–22, 2002, pp. 465–490.
- [24] M. Tüchler, "Design of serially concatenated systems depending on the block length," *IEEE Trans. Commun.*, vol. 52, no. 2, pp. 209–218, Feb. 2004.
- [25] L. Hanzo, T. H. Liew, B. L. Yeap, R. Y. S. Tee, and S. X. Ng, *Turbo Coding, Turbo Equalisation and Space-Time Coding: EXIT-Chart-Aided Near-Capacity Designs for Wireless Channels*, 2nd ed. Hoboken, NJ, USA: Wiley, Mar. 2011.
- [26] L. Kong, S. X. Ng, R. Y. S. Tee, R. G. Maunder, and L. Hanzo, "Reduced-complexity near-capacity downlink iteratively decoded generalized multi-layer space-time coding using irregular convolutional codes," *IEEE Trans. Wireless Commun.*, vol. 9, no. 2, pp. 684–695, Feb. 2010.
- [27] H. V. Nguyen, S. X. Ng, and L. Hanzo, "Irregular convolution and unity-rate-coded network-coding for cooperative multi-user communications," *IEEE Trans. Wireless Commun.*, vol. 12, no. 3, pp. 1231–1243, Mar. 2013.
- [28] S. ten Brink, "Convergence behaviour of iteratively decoded parallel concatenated codes," *IEEE Trans. Commun.*, vol. 49, no. 10, pp. 1727–1737, Oct. 2001.
- [29] B. Medepally and N. B. Mehta, "Voluntary energy harvesting relays and selection in cooperative wireless networks," *IEEE Trans. Wireless Commun.*, vol. 9, no. 11, pp. 3543–3553, Nov. 2010.
- [30] H. Ochiai, P. Mitran, and V. Tarokh, "Design and analysis of collaborative diversity protocols for wireless sensor networks," in *Proc. IEEE VTC Fall*, Los Angeles, CA, USA, Sep. 26–29, 2004, pp. 4645–4649.
- [31] D. Divsalar, S. Dolinar, and F. Pollara, "Serial turbo trellis coded modulation with rate-1 inner code," in *Proc. ISIT*, Sorrento, Italy, Jun. 25–30, 2000, p. 194.
- [32] M. Tüchler, "Convergence prediction for iterative decoding of three-fold concatenated systems," in *Proc. GLOBECOM*, Taipei, Taiwan, Nov. 17–21, 2002, vol. 2, pp. 1358–1362.
- [33] S. X. Ng, J. Wang, M. Tao, L.-L. Yang, and L. Hanzo, "Iteratively decoded variable-length space-time coded modulation: Code construction and convergence analysis," *IEEE Trans. Wireless Commun.*, vol. 6, no. 5, pp. 1953–1963, May 2007.

- [34] R. Y. S. Tee, O. Alamri, S. X. Ng, and L. Hanzo, "Bit-interleaved sphere-packing-aided iteratively detected space-time coded modulation," *IEEE Trans. Veh. Technol.*, vol. 58, no. 1, pp. 493–499, Jan. 2009.
- [35] T. Cover and A. E. Gamal, "Capacity theorems for the relay channel," *IEEE Trans. Inf. Theory*, vol. IT-25, no. 5, pp. 572–584, Sep. 1979.
- [36] J. G. Proakis, *Digital Communications*, 4th ed. New York, NY, USA: Mc-Graw, 2001.
- [37] J. W. Lee and R. E. Blahut, "Generalized EXIT chart and BER analysis of finite-length turbo codes," in *Proc. IEEE Global Telecommun. Conf.*, San Francisco, CA, USA, Dec. 2003, vol. 4, pp. 2067–2072.
- [38] C. Xu, D. Liang, S. X. Ng, and L. Hanzo, "Reduced-complexity non-coherent soft-decision-aided DAPSK dispensing with channel estimation," *IEEE Trans. Veh. Technol.*, vol. 62, no. 6, pp. 2633–2643, Jul. 2013.



Soon Xin Ng (S'99–M'03–SM'08) received the B.Eng. degree (first class) in electronics engineering and the Ph.D. degree in wireless communications from the University of Southampton, Southampton, U.K., in 1999 and 2002, respectively.

From 2003 to 2006, he was a Postdoctoral Research Fellow, working on collaborative European research projects such as SCOUT, NEWCOM, and PHOENIX. Since August 2006, he has been a member of academic staff with the School of Electronics and Computer Science, University of Southampton.

He is involved in the OPTIMIX and CONCERTO European projects, as well as the IU-ATC and UC4G projects. He is currently an Associate Professor of wireless communications with the University of Southampton. He has published over 180 papers and coauthored two John Wiley/IEEE Press books in his fields of interest. His research interests include adaptive coded modulation, coded modulation, channel coding, space-time coding, joint source and channel coding, iterative detection, orthogonal frequency-division multiplexing, multiple-input multiple-output, cooperative communications, distributed coding, quantum error correction codes, and joint wireless-and-optical-fiber communications.

Dr. Ng is a Chartered Engineer and a Fellow of the Higher Education Academy in the U.K.



Yonghui Li (M'04–SM'09) received the Ph.D. degree from Beijing University of Aeronautics and Astronautics, Beijing, China, in 2002.

From 1999 to 2003, he was a Project Manager with Linkair Communication Inc., where he was engaged in the design of physical-layer solutions for the large-area-synchronized code-division multiple-access system. Since 2003, he has been with the Centre of Excellence in Telecommunications, University of Sydney, Sydney, Australia. He is currently an Associate Professor with the School of Electrical and

Information Engineering, University of Sydney. He holds a number of patents granted and pending in his fields of interest. His current research interests include wireless communications, with a particular focus on multiple-input multiple-output, cooperative communications, coding techniques, and wireless sensor networks.

Dr. Li is an Executive Editor for the *European Transactions on Telecommunications*. He has also been involved with the Technical Committee of several international conferences, such as the IEEE International Conference on Communications, the IEEE Global Communications Conference, etc. He was the Australian Queen Elizabeth II Fellow and is currently the Australian Future Fellow.



Branka Vucetic (F'03) received the B.S.E.E., M.S.E.E., and Ph.D. degrees in electrical engineering, from the University of Belgrade, Belgrade, Yugoslavia, in 1972, 1978, and 1982, respectively.

He is currently the Peter Nicol Russel Chair of Telecommunications Engineering with the University of Sydney, Sydney, Australia. During her career, she has held various research and academic positions in Yugoslavia, Australia, the U.K., and China. She has coauthored four books and more than 300 papers in telecommunications journals and conference proceedings. Her research interests include wireless communications, coding, digital communications theory, and machine-to-machine communications.

Prof. Vucetic was elected IEEE Fellow for her contributions to the theory and applications of channel coding.



Lajos Hanzo (F'08) received the M.S. degree in electronics and the Ph.D. degree from Budapest University of Technology and Economics (formerly the Technical University of Budapest), Budapest, Hungary, in 1976 and 1983, respectively; the D.Sc. degree from the University of Southampton, Southampton, U.K., in 2004; and the "Doctor Honoris Causa" degree from Budapest University of Technology and Economics in 2009.

During his 38-year career in telecommunications, he has held various research and academic posts in Hungary, Germany, and the U.K. Since 1986, he has been with the School of Electronics and Computer Science, University of Southampton, where he holds the Chair in Telecommunications. He is currently directing a 100-strong academic research team, working on a range of research projects in the field of wireless multimedia communications sponsored by industry, the Engineering and Physical Sciences Research Council of the U.K., the European Research Council's Advanced Fellow Grant, and the Royal Society Wolfson Research Merit Award. During 2008–2012, he was a Chaired Professor with Tsinghua University, Beijing, China. He is an enthusiastic supporter of industrial and academic liaison and offers a range of industrial courses. He has successfully supervised more than 80 Ph.D. students, coauthored 20 John Wiley/IEEE Press books on mobile radio communications totaling in excess of 10 000 pages, and published more than 1400 research entries on IEEE Xplore. He has more than 20 000 citations. His research is funded by the European Research Council's Senior Research Fellow Grant.

Dr. Hanzo is a Fellow of the Royal Academy of Engineering, The Institution of Engineering and Technology, and the European Association for Signal Processing. He is also a Governor of the IEEE Vehicular Technology Society. He has served as the Technical Program Committee Chair and the General Chair of IEEE conferences, has presented keynote lectures, and has been awarded a number of distinctions. During 2008–2012, he was the Editor-in-Chief of the IEEE Press.